Original article

On the frequency-dependent attenuation in low-frequency mechanical testing of rock samples

Wubing Deng[1,2,3], Igor B. Morozov[4], Li-Yun Fu[1,2,3]*

[1]*State Key Laboratory of Deep Oil and Gas, China University of Petroleum (East China), Qingdao 266580, P. R. China*

[2]*School of Geosciences, China University of Petroleum (East China), Qingdao 266580, P. R. China*

[3]*Laboratory for Marine Mineral Resources, Qingdao Marine Science and Technology Center, Qingdao 266237, P. R. China*

[4]*Department of Geological Sciences, University of Saskatchewan, Saskatoon S7K 5E2, Canada*

Abstract:
In forced-oscillation mechanical testing of rock samples, low-frequency attenuation is traditionally measured by the tangent of the strain-stress phase lag, which is interpreted as the frequency-dependent inverse quality factor. However, such phenomenological parameter only refers to harmonic waves in a homogeneous medium, lacking physical meaning in heterogeneous media or for finite bodies. It depends on specific boundary conditions and becomes insufficient for characterizing fluid-saturated porous rock. It is also sensitive to geometrical spreading, which is poorly known but can be significant in forced-oscillation experiments. To overcome these limitations and uncertainties of quality factor, one can use the temporal attenuation coefficient, a more fundamental quantity directly representing the relative mechanical-energy dissipation rate within the medium. Here, frequency-dependent attenuation coefficient is formulated from calibration experiments with Plexiglas and several published forced-oscillation measurements with fluid-containing porous rocks at variable temperatures. The resulting attenuation coefficient, unlike the quality factor, reveals important attenuation attributes: Effective geometrical attenuation, effective attenuation, relaxation time, and effective viscosity. The effective attenuation is related to the presence of pore fluids or melts, increases with temperature, and decreases with static pressure and pore-fluid viscosity. The effective geometrical attenuation is small in experiments with sandstone but becomes significant in high-temperature, torsional-deformation experiments with olivine aggregates. Unlike the inverse quality factor, the peak in the residual attenuation coefficient yields additional quantitative parameters to characterize the elasticity and internal friction within the rock. This work provides a new way for studying seismic attenuation, which shall be helpful to oil and gas exploration.

1. Introduction

In subresonant measurements of seismic attenuation using rock specimens (Spencer, 1981; Jackson and Paterson, 1993), there exists a striking disparity between the complexity of the measured phenomena and exceedingly simple theoretical models used for data interpretation. The complex and multi-faceted phenomenon of seismic wave attenuation is measured from the phase lag θ between the sinusoidal mechanical stress and average strain (the loss tangent, $Q^{-1} = \tan\theta$) observed for a small rock specimen (Spencer, 1981). At each testing frequency f, Q^{-1} is reported as the key measure of seismic wave attenuation. By deconvolving the measured stress and strain time series, the time- or frequency-dependent "dynamic" modulus for the given type of deformation (denoted $M(t)$ and $M(f)$ here) is also obtained. The noted simplistic theoretical model consists in assuming that the strain-stress phase lag θ and the measured functions $Q^{-1}(f)$, $M(f)$, or $M(t)$ represent some effective rock properties and can therefore be directly related to the material *in situ*.

The assumption of effective material properties $Q^{-1}(f)$

and $M(f)$, which are almost directly measurable in the laboratory, is a powerful hypothesis broadly used in experimental materials science (Lakes, 2009). This hypothesis has originated from early studies of time-dependent linear creep in rock samples (Lomnitz, 1957) and was formalized in the linear viscoelastic theory, which postulated that time-delayed strain-stress relations are inherent in materials (Lakes, 2009). However, the viscoelastic theory only summarizes the above observations by mathematical transformations in time: Using the Boltzmann's linearity principle, differential or integral operators, fractional derivatives in time, Zener's or similar equations, or assumed kinetic equations for material properties (Nowick and Berry, 1972). Nonetheless, such time-based descriptions are only appropriate for limited cases in which time is the only independent variable, such as low-frequency measurement with a small rock sample. In contrast to this model, physics generally teaches that at a single point within a real heterogeneous medium, there exists no definite relation between the time histories of any parameters (density, strain, stress, temperature, etc.), but these histories are determined by spatial interactions with adjacent areas in the form of waves or flows. Therefore, there also exist no material-specific spectra $Q^{-1}(f)$ or $M(f)$ and no fixed time-dependent modulus function $M(t)$.

Thus, the observed $Q^{-1}(f)$ or $M(f)$ are only empirical relations measured in certain experiments such as creep under certain selected boundary conditions and for certain wave modes (standing or traveling, P, S, extensional, surface, tube, etc.). For fluid-saturated porous rock, physical limitations of the viscoelastic paradigm were noted long ago. For example, Geertsma and Smit (1961) emphasized that viscoelastic approximations only refer to freely traveling primary-wave modes in uniform media, but they become invalid for reflections. White (1986) pointed out "a common fallacy" of assuming viscoelastic relations between dynamic moduli measured in porous rock samples, but this fallacy still persists in many experimental studies today.

For subresonant forced-oscillation laboratory experiments, the measured $Q^{-1}(f)$ and $M(f)$ spectra are affected by many experimental factors: Sample dimensions, layering, pore-fluid content, heterogeneity, granularity and saturation, thermal regime and boundary conditions. Morozov et al. (2018) showed that the bulk-modulus attenuation (Q^{-1}) peak measured in a 8 cm long sandstone specimen by Pimienta et al. (2015a) is about ten times greater than the Q^{-1} peak measured in a traveling wave at the same frequency. "Viscoelastic" Q^{-1} peaks may even be caused by pore-fluid flows occurring outside of the rock specimen, such as the "drained-to-undrained transition" artifacts caused by the dead volume of the measurement apparatus (Pimienta et al., 2015b; Morozov et al., 2018; Tan et al., 2020). As shown in the present paper, by focusing on the frequency-band averaged attributes (effective geometrical attenuation γ, effective attenuation q_e, relaxation time τ_e, and effective viscosity η_e) rather than solely on the peaks of $Q^{-1}(f)$, true attenuation properties of the material become clearer, and material properties can be constrained more accurately.

In addition to the reliance on assumed time- or frequency-dependent material properties, the conventional parameterization of rock-physics measurements by functions $Q^{-1}(f)$ or $M(f)$ leads to two additional methodological difficulties, which are nevertheless often unnoticed. First, the theoretical viscoelastic modulus M and the corresponding Q^{-1} refer to the so-called Cauchy (surface) stresses, which are only a part of the forces acting within the medium. For example, wave attenuation within porous fluid-saturated reservoir rock or soil is often dominated by body-force (Darcy drag) friction, which is not included in the viscoelastic Cauchy stress. Thus, the moduli measured for porous-rock samples are not viscoelastic (Geertsma and Smit, 1961). Similar body forces should also be dominant within a layered reservoir or near the free surface or water table. Inertial body forces represent another type of non-viscoelastic phenomena significant in near Biot's characteristic frequency, but they are usually insignificant at seismic frequencies (Deng et al., 2024).

Another important issue with the $Q^{-1}(f)$ parameterization of attenuation measurements is related to its disregard of geometrical spreading (Morozov, 2008, 2010a). It is often thought that geometrical spreading (GS) is absent in subresonant laboratory experiments merely because there are no traveling waves in them. On the contrary, as shown in this paper, an equivalent of GS is possible, measurable, and also significant in some laboratory experiments (i.e., the melt-bearing specimens of synthetic polycrystalline olivine aggregates by Jackson et al. (2004)), although the sample is much smaller (centimeter-scale) than the wavelength (tens to hundreds of meters) of the sinusoidal oscillations.

The ultimate goal of laboratory experiments consists in learning about the properties of seismic waves traveling or reflecting within the earth, which can be better achieved by using the frequency-dependent temporal attenuation coefficient χ. For traveling waves, the principal measures of attenuation are the spatial attenuation coefficient $\alpha(f)$ and the temporal attenuation coefficient $\chi = \alpha/c$, where c is the wave velocity (Aki and Richards, 2002). These quantities characterize the amplitude and energy decay rates within the wave and also yield secondary attributes such as the displacement-acceleration phase lag or Q^{-1}. For rock samples in frequency-domain forced-oscillation measurements, attributes α and χ are not easily accessible, but they can often be extracted as described in section 2. The extracted χ allows making significant new observations. Instead of strong variations of Q^{-1} with frequency, $\chi(f)$ shows a nonzero limit at low frequency and a systematic increase with frequency related to wave attenuation. New parameters γ, q_e and τ_e are obtained, which lead to instructive links to the physical properties of the tested material. In particular, a new material property of effective solid viscosity is estimated and denoted η_e.

In section 3, the $\chi(f)$ data parameterization is illustrated on four applications to forced-oscillation mechanical testing of rock samples. To explore a variety of material types and frequency-dependent behaviors, published extensional-deformation measurements with fluid-saturated Berea sandstone at variable temperatures are revisited (Mikhaltsevitch et al., 2016), similar experiments with Plexiglas at variable confining pressures, measurements of bulk and shear moduli of bi-

tumen sand (Spencer et al., 2013), and torsional deformations of melt-free and melt-bearing specimens of synthetic poly-crystalline olivine aggregates (Jackson et al., 2004). In each of these examples, quantitative correlations of the measured $\chi(f)$ dependencies with pore fluids, temperatures, fluid content, and other conditions of the experiments are demonstrated. In section 4, the $\chi(f)$ and $Q^{-1}(f)$ parameterizations are further compared and their relations to the internal structure of the material are discussed. In this section, further discussions on the new parameters γ, q_e and τ_e will also be addressed.

2. Temporal attenuation coefficient

Let us start with the definition of the attenuation coefficient χ for a wave. Since the measured attenuation and disper-sion spectra are usually related by the Kramers-Krönig rela-tions (for example, the differential relation $d(\ln M)/d(\ln f) \approx 2Q^{-1}/\pi$; Mikhaltsevitch et al., 2016), it is sufficient to focus on attenuation. For a traveling or standing wave, the time- and frequency-dependent amplitude at time t and frequency f can be expressed as:

$$A(f,t) = G(f,t)\exp\left[-\int \chi(f,\tau)d\tau\right] \quad (1)$$

where $G(f,t)$ is the GS possibly including the source signa-ture, and time integration is performed along the ray path. Eq. (1) represents a perturbation or scattering-theory approx-imation, in which $G(f,t)$ serves as an unperturbed solution for the elastic wave, and $\chi(f,t)$ is the attenuation (damping) coefficient.

Eq. (1) for wave amplitude is often written by expressing χ through the Q-factor as (Aki and Richards, 2002):

$$A(f,t) = G(f,t)\exp\frac{-\pi ft}{Q} \quad (2)$$

Thus, Q^{-1} is derived from the attenuation coefficient as:

$$Q^{-1}(f,t) = \frac{\chi(f,t)}{\pi f} \quad (3)$$

Note that both χ and Q are generally functions of not only frequency but also time t. In attenuation experiments, homo-geneous media are usually assumed, and time dependencies of these quantities are disregarded. Nevertheless, Eq. (3) shows that viewing χ and Q as functions of frequency only (as done in the viscoelastic model) is valid only for quasi-homogeneous media (Morozov and Ahmadi, 2015). One should also note that through dividing χ by frequency f, Q may down-weigh the high-frequency effect of attenuation and creates an artifact (near-zero Q) at low frequencies.

The attenuation coefficient χ has a straightforward physical meaning of the relative rate of amplitude decrease in an oscil-latory process. Because the energy of an oscillation or energy flux in a wave is proportional to the squared amplitude A^2, quantity 2χ represents the relative rate of energy dissipation per unit volume and time. Therefore, χ is practically useful and directly observable from the rate of amplitude decay in an arbitrary free oscillation or wave: $\chi = -\partial\ln(A/G)/\partial t$.

In contrast to the general mechanical-energy related mean-ing of χ, the quality factor Q (Eq. (3)) is specialized to

harmonic oscillations in which the displacement is of the form $u(f,t) = A(f,t)\exp(-i\omega t)$. The amplitude decrease by Eq. (1) leads to an imaginary shift of this frequency as $\omega^* = \omega - i\chi$. Note that this frequency shift shows another simple meaning of the attenuation coefficient χ. For this damped os-cillation, the tangent of the phase lag between the displacement and acceleration equals $\tan\delta = -\text{Im}(\omega^{*2})/\text{Re}(\omega^{*2}) \approx 2\chi/\omega$, which equals Q^{-1} in Eq. (3). Because of this relation to χ, the phase lag is used in forced-oscillation attenuation measurements (Jackson and Paterson, 1993), in which it is difficult to measure the weak energy dissipation rate directly.

Because of the division by f in Eq. (3), the Q^{-1} is ex-tremely sensitive to the frequency dependence of $\chi(f)$ at low frequencies. When relying on a phase-lag Q^{-1} as attenuation property of rock, it is assumed that χ must be proportional to f at low frequencies. Thus, the premise of the $Q(f)$ parameterization is that quantity $\ln(A/G)$ increases not merely with t but with the number of oscillation periods equal the time-frequency product ft. However, this premise is often wrong in practice. Most field observations with body, surface, and coda waves (Morozov, 2008, 2010a, 2010b; Morozov et al., 2018), models of thermoelastic phenomena and some laboratory experiments (section 3) show that χ may behave differently at low frequencies, and this behavior cause spurious variations of $Q(f)$. For example, a nonzero $\lim_{f\to 0}\chi = \gamma$ due to an under-corrected GS leads to a hyperbolic increase of $Q^{-1} \approx \gamma/\pi f$ at low frequencies, or thermoelastic friction may lead to $\chi \approx const\cdot\sqrt{f}$ and $Q^{-1} \approx const/\sqrt{f}$ (Landau and Lifshitz, 1986). In earthquake seismology, such Q^{-1} steeply increasing toward low frequencies is often reported in and interpreted as manifestation of a "frequency dependence of Q" for the earth (Anderson et al., 1977). Nevertheless, this depen-dence is largely due to the instability of the Q parameterization with respect to the uncertainties of $\chi(f)$ at low frequencies (Morozov, 2008, 2010a).

The concept of attenuation coefficient χ also helps clar-ifying a popular misconception about the meaning of band-limited seismic attenuation. For example, global Q models represent the Earth's mantle as a combination of absorption bands with power-law $Q^{-1}(f)$ transitions across their flanks (Anderson et al., 1977). In laboratory rock physics, it is also believed that seismic attenuation is concentrated near certain relaxation frequencies at which peaks in $Q^{-1}(f)$ occur (Jack-son et al., 2004; Pimienta et al., 2015b). The standard linear solid (Zener's) model is often used to illustrate this band-limited behavior (Lakes, 2009). In this model, the frequency dependence of the phase-lag Q^{-1} equals:

$$Q^{-1}(f) = 2Q_{peak}^{-1}\frac{\dfrac{f}{f_{peak}}}{1+\left(\dfrac{f}{f_{peak}}\right)^2} \quad (4)$$

Peaks of $Q^{-1}(f)$ correspond to the maximum phase lags and occur at frequencies f_{peak} at which $\chi(f)$ satisfies equa-tion $d(\chi/f)/df = 0$, which simplifies to $d\chi/df = \chi/f$, or $d(\ln\chi)/d(\ln f) = 1$. Thus, Q_{peak}^{-1} also corresponds to points with $45°$ slopes on log-log $\chi(f)$ plots. Below and above this
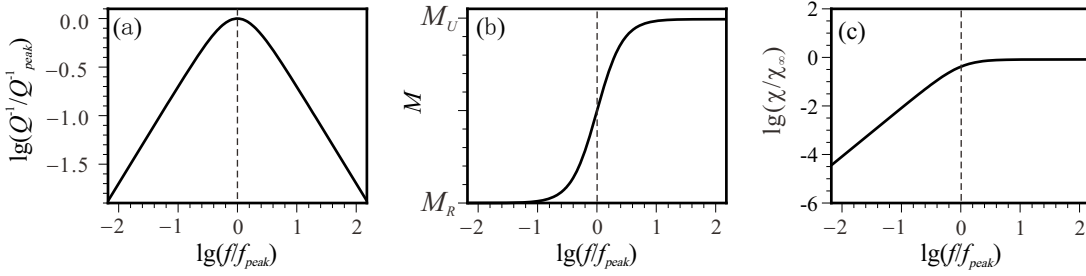
Fig. 1. Observable properties of the standard linear (Zener's) solid: (a) Phase-lag Q^{-1}, (b) empirical modulus, and (c) attenuation coefficient χ. M_R and M_U are the relaxed and unrelaxed elastic moduli of the standard linear solid, respectively, $Q_{peak}^{-1} = (M_U - M_R)/(2\sqrt{M_R M_U})$ is the peak value of $Q^{-1}(f)$, f_{peak} is the frequency at which this peak occurs, and $\chi_\infty = 2 f_{peak} Q_{peak}^{-1}$ is the asymptotic level of attenuation at infinite frequency.

peak, $Q^{-1}(f)$ decreases to zero as f and $1/f$, respectively (Fig. 1(a)), and the dynamic modulus shows the characteristic plateaus (Fig. 1(b)). However, do these low values of Q^{-1} mean that wave attenuation is also weak at both $f \ll f_{peak}$ and $f \gg f_{peak}$? Evaluation of the attenuation coefficient $\chi = \pi f Q^{-1}$ shows that this is not so (Fig. 1(c)). The mechanical-energy dissipation rate (energy absorption) is not limited to the vicinity of fpeak but continuously increases with frequency (Fig. 1(c)). At low frequencies, the absorption rate increases as $\chi \propto f^2$, which is slower than if interpreting $Q^{-1}(f)$ as the wave attenuation rate. At frequencies $f > f_{peak}$, the attenuation coefficient continues to increase and approaches an asymptotic level $\chi_\infty = 2 f_{peak} Q_{peak}^{-1}$, which is twice the level of χ at the relaxation frequency (Fig. 1(c)). That is to say, f_{peak} are not frequencies at which the strongest energy dissipation occurs. Therefore, it is indeed that, as shown in Fig. 1, the $\chi(f)$ is more accurate and reveals properties not seen in the $Q(f)$ form.

2.1 Material-property parameters in $\chi(f)$ dependencies

In several earlier studies (Morozov, 2008, 2010a, 2010b; Ahmadi and Morozov, 2013; and other papers by these authors), frequency-dependent attenuation coefficients $\chi(f)$ were derived for a broad variety of experiments in observational and exploration seismology. It was shown that in contrast to the often-strong variations of $Q^{-1}(f)$, values of $\chi(f)$ vary less and exhibit systematic increases with frequency. Frequency dependencies of $\chi(f)$ can be naturally classified into several functional forms using the Taylor series of $\chi(f)$ at low frequencies. Using the angular frequency ω, an extended form of this classification is:

$$\chi(\omega) = \gamma + \frac{q_e}{2}\omega + \frac{\tau}{2}\omega^2 + \tilde{\chi}(\omega) \tag{5}$$

The different terms in this relation correspond to material properties and (potentially) features of the experimental design. These terms can be interpreted as follows:

1) The zero-frequency intercept defined as $\gamma = \lim_{f \to 0} \chi$ represents the effective GS. More precisely, this GS is the frequency-independent deviation $\exp(-\gamma t)$ of the zero-

attenuation limit of the present structure relative to the selected reference model $G(f,t)$ (Eq. (1)) (Morozov, 2008, 2010a).

2) The dimensionless parameter q_e describes a linear trend with respect to ω. By analogy with the conventional quality factor, Morozov (2008) called parameter $Q_e = 1/q_e$ the (frequency-independent) effective Q. The nonzero q_e can be expected for two reasons: (a) As a simple empirical form commonly used in constant-Q attenuation measurements, or (b) as a result of dry (Coulomb) friction between rock grains (Coulman et al., 2013). For forced-oscillation attenuation measurements, q_e may also include a contribution from calibration of the measured phase lags.

3) The quadratic term proportional to ω^2 defines a characteristic time constant τ. For a homogeneous rock sample or medium, τ is the relaxation time with respect to a sudden increase of stress and related to the (effective) linear solid viscosity η_e of the rock and its modulus M as $\tau = \eta_e / M$ (Coulman et al., 2013). Viscosity means internal friction with forces proportional to displacement or strain rates. From the most general principles of mechanics, viscous friction is expected in all materials or media including solids (Landau and Lifshitz, 1986). For rock, solid viscosity can be produced by fluid flows (Deng and Morozov, 2016), surface tension, movement of grains and dislocations, Brownian motion, thermoelastic, electrochemical, and other effects. For example, the numerical results by Gurevich et al. (2010) shows that the squirt-flow mechanism within seismic frequency can be well explained by the parameter τ.

4) The residual term $\tilde{\chi}(\omega)$ denotes the attenuation spectrum with no broad-band trend with frequency. Peaks and troughs in this attenuation spectrum can be produced by deformations of the internal structure within rock, such as relative shifts of groups of grains, displacements on microcracks and dislocations, deformations of pores or patches of fluid saturation, temperature variations and heat flows, wetting, and other effects (Chen et al., 2021). Since parameter 2χ directly measures the mechanical-energy dissipation rate, peaks in $\tilde{\chi}(f)$ should be more

significant than those of $Q^{-1}(f)$ in practical modeling of seismic waves.

Earthquake and controlled-source field studies (references in the preceding paragraph) show that parameters γ and q_e have remarkably consistent values correlated with the layering, tectonic types, and ages of the crust. Parameter τ was not considered in those studies. The first three terms in Eq. (5) usually dominate the data, and the residual variations $\tilde{\chi}(\omega)$ are relatively insignificant (Morozov, 2008, 2010a). The pair of parameters (γ, q_e) effectively replaces parameters Q_0 and η in the power law $Q(f) = Q_0 f^\eta$ that is often used to describe the frequency-dependent Q. As shown in section 3, in the laboratory observations, parameters γ and q_e also account for most of the data, and they exhibit clear sensitivity to physical properties of the samples.

Parameters τ and q_e are caused by similar physical effects (different forms of solid viscosity or thermoelasticity) and describe similar increases of the attenuation coefficient with frequency. Because of this similarity, these parameters may be difficult to separate in real data. To absorb the trade-off between these parameters, another characteristic ("effective") time τ_e is defined as:

$$\tau_e = \tau + \frac{q_e}{f_0} \tag{6}$$

where f_0 is the characteristic frequency of the experiment, such as the dominant frequency or middle of the measured frequency band. Using this time constant, the characteristic solid viscosity is estimated as $\eta_e = M\tau_e$ (Coulman et al., 2013). This parameter is a useful material property related to internal friction and seismic attenuation, and it can be estimated from laboratory experiments.

Thus, the proposed parameterization of forced-oscillation data reveals two or three attenuation attributes (γ, q_e, and potentially τ_e) characterizing the entire frequency band. Note that these parameters are difficult to see in the raw $Q^{-1}(f)$ data. The residual quantity $\tilde{\chi}(f)$ can be interpreted similarly to the conventional $Q^{-1}(f)$, i.e., as a combination of relaxation peaks, which give additional characteristic times to the description of the medium. In empirical viscoelastic models, frequencies of these peaks are treated as independent material properties (relaxation times; Jackson et al., 2004). In rigorous continuum-mechanics models, these characteristic times represent solutions of a generalized eigenvalue problem involving combinations of multiple viscous and elastic parameters of the medium (Morozov et al., 2018, 2020; Chen et al., 2021).

Compared with the conventional $Q^{-1}(f)$ spectra, $\chi(f)$ dependencies reveal additional and practically valuable information: A quantitative measure of the effective GS (denoted γ), effective attenuation q_e and viscosity η_e, which can also be represented by the characteristic relaxation time τ_e. Quantity γ is an important parameter of the experimental setup, and q_e, η_e, and τ_e are applicable to waves traveling in a medium of the same material. By contrast, the complete $Q^{-1}(f)$ spectrum may not be directly transportable to wave environment because of these different attenuation phenomena being intermixed in it (Morozov et al., 2018). In $Q(f)$ form, it is practically impossible to see the gradual trend of attenuation $\chi(f)$ increasing with

frequency, and it is also impossible to see the zero-frequency limit of attenuation effects. Thus, the $\chi(f)$ is more accurate it reveals properties not seen in the $Q(f)$ form.

2.2 Effective geometrical spreading

By using the Taylor expansion at low frequencies, the $\chi(f)$ has been decomposed into four terms as shown in Eq. (5). Coefficients of the first three terms reflect the frequency-band averaged attenuation attribute of the rock and have specific physical meanings. Among these, the parameter γ represents the effective GS analogue to the conventional GS. Leaving aside the historical origins of this term in geometrical optics, the GS refers to the behavior of a given mechanical system in the limit of zero attenuation (i.e., zero mechanical-energy dissipation) within it (Morozov and Ahmadi, 2015). In this paper, the term GS is used in this sense. For example, for a rock sample in a laboratory apparatus, the effective GS consists in deformation of a sample having the same dimensions and elastic properties but completely free from internal friction, i.e., elastic.

For both traveling waves and rock samples, the zero-attenuation limit is always hypothetical because no elastic equivalents exist for real rocks or earth media. Nevertheless, this hypothetical limit is the key element of all attenuation studies, and no Q can be defined without it. In laboratory experiments, a standard aluminum cylinder is usually used as such a perfectly elastic reference (Jackson and Paterson, 1993), but this is still not completely equivalent to the target sample being elastic. In the viscoelastic theory, the elastic limit is postulated mathematically, as the instantaneous response after a step of loading (Lakes, 2009)-but this response is also unavailable in experiments with waves and with forced-oscillation loading in the laboratory. Note that for traveling waves, the conventional GS is also typically "non-geometrical" and taken in forms unrealizable by wavefront geometries, such as dependencies $G(t) \propto t^{-\nu}$ with ν not equal 0.5 or 1. This effective GS includes ray bending, multipathing, scattering, and reflections and mode conversions within heterogeneous structures (Morozov, 2008, 2010a). In seismic coda studies, the commonly considered GS limit is similarly hypothetical and consists of assuming straight rays and spherical wavefronts (Aki and Chouet, 1975), which are impossible in real crustal and mantle structures.

Despite the hypothetical character of the pure elastic GS limit, this limit can readily be measured from the frequency dependence of $\chi(f)$. Because the attenuation coefficient usually increases with frequency, the GS limit can be assessed by the zero-frequency limit of the attenuation coefficient: $\gamma = \chi(f \to 0)$ (Morozov, 2008, 2010a).

For a harmonic wave spreading within an elastic medium, the GS is described by empirical laws giving the decrease of the recorded amplitude or energy with propagation time. This GS may depend on the wave frequency (Yang et al., 2007), which is analogous to the behavior of a rock sample described further. Similar to wave spreading, an ideal elastic rock sample undergoing forced oscillations will generally dissipate mechanical energy with time, and this process can be designated
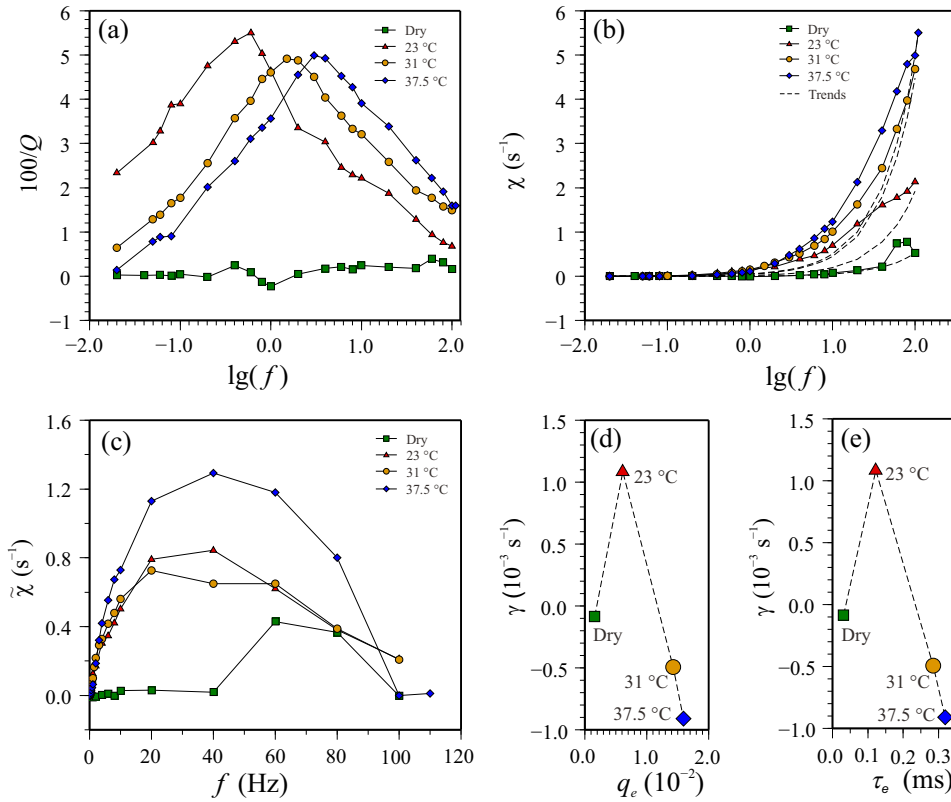
Fig. 2. Young's modulus measurements in a dry and glycerol-saturated sample of Berea sandstone (Mikhaltsevitch et al., 2016) at temperatures 23, 31 and 37.5 °C (legends and labels): (a) Measured $Q^{-1}(f)$; (b) the same measurements in $\chi(f)$ form; dashed lines show the smooth trends due to the first three terms in Eq. (5); (c) residual $\tilde{\chi}(f)$ dependencies; (d) cross-plot of values q_e and γ for the four tests; (e) cross-plot of η_e and γ.

as the effective GS in the experiment. For example, frequency-independent mechanical-energy dissipation can be caused by scattering on small-scale heterogeneities (Morozov, 2011) or by thermoelastic heating of the sample.

In summary, the effective GS is similar to the conventional GS observed in the field because both are the zero-frequency limit of wave amplitude decay and are influenced by small-scale scattering (Morozov, 2011) and thermoelasticity. However, conventional GS is also affected by wave geometry, such as ray shapes and wavefront curvatures. In contrast, the effective GS in a small sample is solely due to small-scale scattering and thermoelasticity. Thus, the effective GS measured in the lab likely represents a lower bound on the GS seen in field data.

3. Examples

In the following subsections, attenuation observations from four published forced-oscillation laboratory experiments are reprocessed in the same way (Fig. 2). First, the reported dependencies such as in Fig. 2(a) are transformed into the attenuation coefficient $\chi(f)$ using Eq. (3) (Fig. 2(b)). Then, the trend represented by the first three terms in Eq. (3) is subtracted from the data, leaving the frequency-dependent structural response $\tilde{\chi}(f)$ (Fig. 2(c)). Note that due to the removal of the broadband trend, it is convenient to plot the

variations of $\tilde{\chi}(f)$ on a linear frequency scale (Fig. 2(c)). Because peaks of $Q^{-1}(f)$ occur at low frequencies f_{Qpeak} (e.g., below ~3 Hz in Fig. 2(a)), the corresponding variations of $\chi(f_{Qpeak})$ are only about 10% of the $\tilde{\chi}(f)$ maxima (Fig. 2(c)). Finally, the values of γ, q_e, and η_e are compared for the different conditions of the experiments (Figs. 2(d) and 2(e)).

When extracting the broadband trend due to parameters γ, q_e, and η_e (Eq. (5)), the trend line is traced through the lower values of $\chi(f)$ data (e.g., Fig. 2(b)), so that the residual is mostly positive. This type of fitting the background trend means that the peak values are expected to be non-negative ($\tilde{\chi}(f) \geq 0$) and describe mechanical-energy dissipation, similarly to the usually expected relation $Q^{-1} \geq 0$. Such type of fitting of the $\chi(f)$ data is implemented by an iterative least-squares inverse with larger weights assigned to the data with negative residuals $\tilde{\chi}(f)$. Finally, if the expected constraint $\tau \geq 0$ is violated (i.e., the least-squares inverse identifies a $\chi(f)$ trend with downward curvature), the solution is discarded, and the curve fitting is repeated with fixed $\tau = 0$ (Eq. (5)). Such cases are interpreted as linear viscosity being unmeasurable from the data.

3.1 Glycerol-saturated sandstone at variable temperatures

Many forced-oscillation attenuation measurements have been conducted in sandstones. As an example, the results reported by Mikhaltsevitch et al. (2016) for several sandstone samples at three temperatures are used. The data were obtained from an electronic supplement to that paper. The principal objective of Mikhaltsevitch et al. (2016) was to investigate the Kramers-Krönig (causality) relations between the empirical Young's modulus and the associated phase-lag $Q^{-1}(f)$. Causality must be automatically satisfied in any experiment of such kind, and therefore it presents a useful tool for checking consistency of the experiment but do not constrain properties of the material. In this section, the $Q^{-1}(f)$ data for Berea sandstone (sample D) from Mikhaltsevitch et al. (2016) is utilized to investigate its attenuation properties. The sample was measured in a dry state at temperature 23 °C and after glycerol saturation at temperatures 23, 31 and 37.5 °C (Fig. 2(a)).

Evaluation of the attenuation coefficients $\chi(f)$ from the reported $Q^{-1}(f)$ (Eq. (3)) shows that they are dominated by broadband upward trends (dashed lines in Fig. 2(b)). Only for dry sample with weak attenuation, the deviation of $\chi(f)$ from the estimated trend between 60 to 100 Hz is comparable to the trend terms (dashed lines in Fig. 2(b)). The trends are dominated by linear terms related to parameter q_e, with $q_e \approx 1.6 \times 10^{-3}$ for dry sample and 6.1×10^{-3}, 1.4×10^{-2}, and 1.6×10^{-2} for glycerol-saturated sample at temperatures 23, 31 and 37.5 °C, respectively (Fig. 2(d)). As expected, attenuation q_e is the lowest for the dry sample and much higher for the saturated cases. Attenuation q_e also increases with temperature for the fluid-saturated sample (Fig. 2(b)).

Because the viscosity of glycerol decreases by about three times across the measured temperature range (Cheng, 2008), the increase of average attenuation q_e coincides with decreasing pore-fluid viscosity. This observation may appear to contradict the intuitive expectation that a more viscous pore fluid should lead to stronger wave attenuation. However, this apparent contradiction is easy to explain. Most of the wave energy is located above frequencies f_{peak} of the peaks, and at frequencies $f > f_{peak}$, the measured $Q^{-1}(f)$ increases with temperature (Fig. 2(a)). Thus, with decreasing pore-fluid viscosity (increasing temperatures), the relaxation peaks shift to higher frequencies (Fig. 2(a)), the mobility of the pore fluid at any fixed testing frequency $f > f_{peak}$ increases, and consequently the dissipated mechanical-energy flux also increases. Fig. 1(c) (attenuation coefficient $\chi_\infty = 2f_{peak}Q^{-1}_{peak}$) also shows that wave attenuation increases proportionally to f_{peak}. A similar trend of positive temperature-attenuation correlation is shown in the "3.4 Melt-bearing olivine aggregates" subsection. Note that for water saturation, the pore fluid viscosity would be about 1,000 times lower and the peaks of $Q^{-1}(f)$ would be located at about 1,000 higher frequencies and above the seismic band. Therefore, for water saturation, the correlation between the viscosity of the pore fluid and the observed wave attenuation should be positive, and the attenuation should decrease with temperature.

In contrast to most field studies (Morozov, 2008, 2010a, 2010b; Ahmadi and Morozov, 2013), the geometrical-spreading parameter γ has an insignificant effect on the present laboratory data (Fig. 2(b)). The characteristic time equals $\tau_e \approx 3.2 \times 10^{-5}$ s (Eq. (6)) for the dry sample and increases with temperature from $\tau_e \approx 13.2 \times 10^{-4}$ to 3.2×10^{-4} s for the glycerol-saturated sample (Fig. 2(e)). Using the Young's modulus value $E \approx 22$ GPa (Mikhaltsevitch et al., 2016), this τ_e corresponds to solid viscosity $\eta_e \approx 7$ MPa·s for dry sample and $\eta_e \approx 27$, 63, and 70 MPa·s in glycerol-saturated states at 23, 31 and 37.5 °C, respectively. These values are within the range of estimates of solid viscosity for sandstone (Morozov et al., 2018; Chen et al., 2021), although in those studies, somewhat different viscosities related to relaxation peaks of $Q^{-1}(f)$ were found, and the average viscosity η_e was not considered.

The detrended attenuation coefficient $\tilde{\chi}(f)$ for the dry and glycerol-saturated states of Berea sample D by Mikhaltsevitch et al. (2016) is shown in Fig. 2(c). Characteristic attenuation peaks are clearly seen in these data. In dry sandstone, there is a peak between 40 and 100 Hz, which may potentially be due to thermoelastic effects in grainy rock (Landau and Lifshitz, 1986). With glycerol saturation, the peaks are shifted to lower frequencies of about 20-60 Hz and broaden. Since these peaks cover the entire measured frequency range, they likely represent not some specific relaxation mechanisms within the sample but a nonlinear attenuation different from the terms proportional to ω and ω^2 in Eq. (5).

Interestingly, the peaks of $\tilde{\chi}(f)$ do not shift with reducing glycerol viscosity (increasing temperatures). Therefore, the progression of $Q^{-1}(f)$ peaks with increasing temperature (Fig. 2(a)) appears to be caused by the increase of the average attenuation q_e or changes in nonlinear attenuation rather than shifting of the relaxation peaks in $\tilde{\chi}(f)$. This observation confirms the suggestion by Morozov et al. (2020) that the peak values of $Q^{-1}(f)$ represent the elastic structure of the material. The peaks or non-quadratic patterns of $\chi(f)$ could also be caused by some interactions on the scale of the whole sample or measurement apparatus, analogous to the drained-to-undrained transition mentioned in the "Introduction" section.

3.2 Bitumen sand

Fig. 3(a) shows attenuation master curves derived by Spencer et al. (2013) for frequency-dependent bulk and shear moduli of Ells River bitumen sand with residual air in the pores. Measurements of empirical Young's moduli and Poisson's ratios were conducted at temperatures 5, 16, 22, 25, 35 and 48 °C. These measurements were transformed into the bulk and shear moduli using elastic-moduli relations and scaled in frequency so that the results fell onto common curves at reference temperature 5 °C (Spencer et al., 2013). These transformations resulted in nonzero $Q^{-1} \approx 0.03$ at the lowest frequencies of about 0.3 mHz and decreasing to about 1 mHz for the bulk modulus and 70 mHz for shear modulus (Fig. 3(a)). The inferred shear modulus Q^{-1} is negative near this frequency, which was a nonphysical result from the viewpoint of the viscoelastic model (Spencer 2013). However,
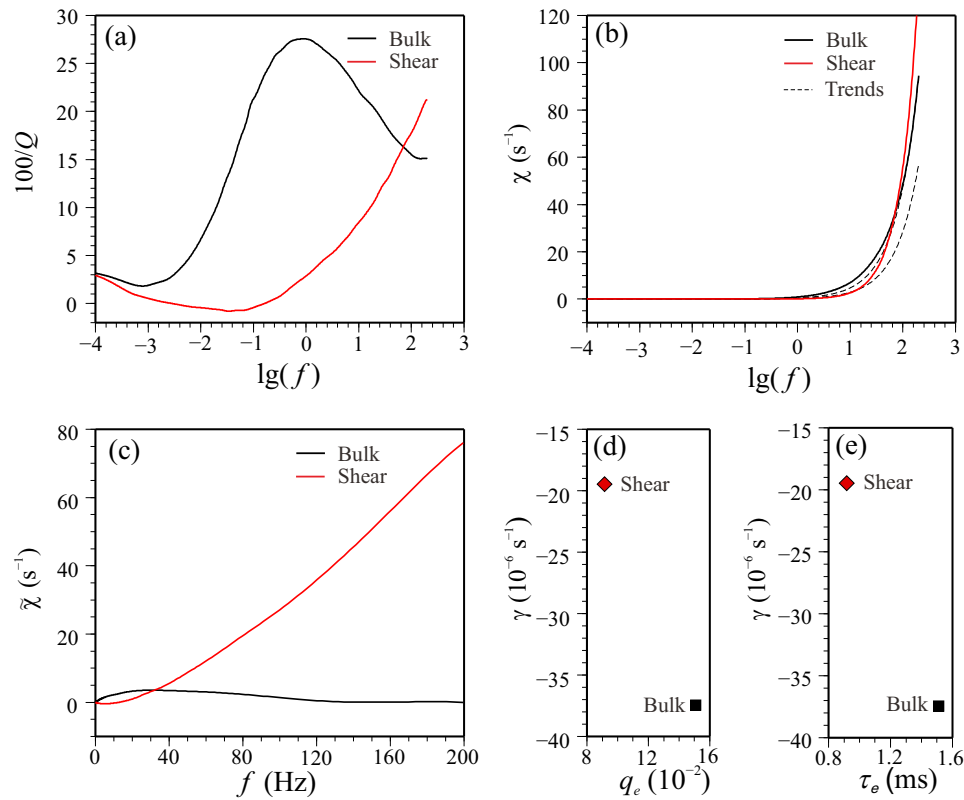
Fig. 3. Temperature-corrected master curves for attenuation of empirical moduli for bitumen sand (Spencer et al., 2013). Bulk and shear deformation data are indicated in the legends and labels. Panels (a) to (e) are as in Fig. 2.

for the present study and likely for most practical applications, this non-viscoelastic behavior at extremely low frequencies has a negligible effect on wave attenuation (Fig. 3(b)).

Similar to the case in Fig. 2, the attenuation coefficient $\chi(f)$ in bitumen sand is dominated by the linear effective-attenuation term (Eq. (5); Fig. 3(b)). For bulk attenuation, $q_e \approx$ 0.15 (Fig. 3(d)), which is about ten times larger than the q_e for glycerol-saturated sandstone (preceding subsection). For shear deformation, the attenuation is weaker and equal $q_e \approx 0.09$ (Fig. 3(d)). When transformed into the characteristic (relaxation) times using Eq. (6), these values give $\tau_e \approx 1.5$ ms for bulk deformation and $\tau_e \approx 0.9$ ms for shear deformation (Fig. 3(e)). Using the low-frequency bulk and shear moduli from Spencer et al. (2013), these values correspond to solid viscosities $\eta_e \approx 1.8$ MPa·s for bulk deformation and $\eta_e \approx$ 0.9 MPa·s for shear. Thus, the attenuation and viscosity are larger for bulk than for shear deformation, which appears to be the common relation in the exploration frequency range.

Figs. 3(b) and 3(c) also show that a significant part of the shear-wave $\chi(f)$ is not included in the trend accounted for by parameters q_e and η_e. Therefore, the shear-wave attenuation in bitumen sands likely requires nonlinear viscosity with non-quadratic terms in $\chi(f)$. For bulk attenuation, the term $\tilde{\chi}(f)$ shows a broad peak with maximum at about 30 Hz (Fig. 3(b)), which is similar to the case of sandstone. Because this peak covers most of the available frequency range, it could also be explained by nonlinear attenuation or some effects occurring on the scale of the whole sample or measurement device.

Parameters γ are very small (about $(2-4) \times 10^{-5}$ s^{-1}, Fig. 3(d)) and have little impact on the data, with small negative values due to the negative slopes of Q^{-1} described at the beginning of this subsection.

3.3 Plexiglas

Attenuation measurement equipment is often tested by measuring dynamic frequency-dependent moduli in Plexiglas (polymethyl methacrylate (PMMA) plastic) cylinders (Lakes, 2009; Tisato et al., 2010). Fig. 4(a) shows results of such Young's modulus attenuation measurements at room temperature and axial confining pressures 7 and 15 MPa by Mikhaltsevitch et al. (2016). In contrast to the sandstone or bitumen sand samples in the preceding examples, $Q^{-1}(f)$ values for Plexiglas increase near continuously across the entire frequency range, and the rate of this increase reduces with confining pressure. Note that in earlier measurements at ambient pressure (page 210 in Lakes (2009); Tisato et al., 2010), the Q^{-1} was much larger ($Q^{-1} \approx 0.08$), and $Q^{-1}(f)$ exhibited a pronounced peak near 3 Hz. These peaks were interpreted as due to thermoelastic effects (Coulman et al., 2013). It appears that application of confining pressure reduces the measured Q^{-1} and removes the peak in $Q^{-1}(f)$ or shifts this peak to much higher frequencies. Possible causes for these differences need to be investigated experimentally and modeled using thermomechanical models.
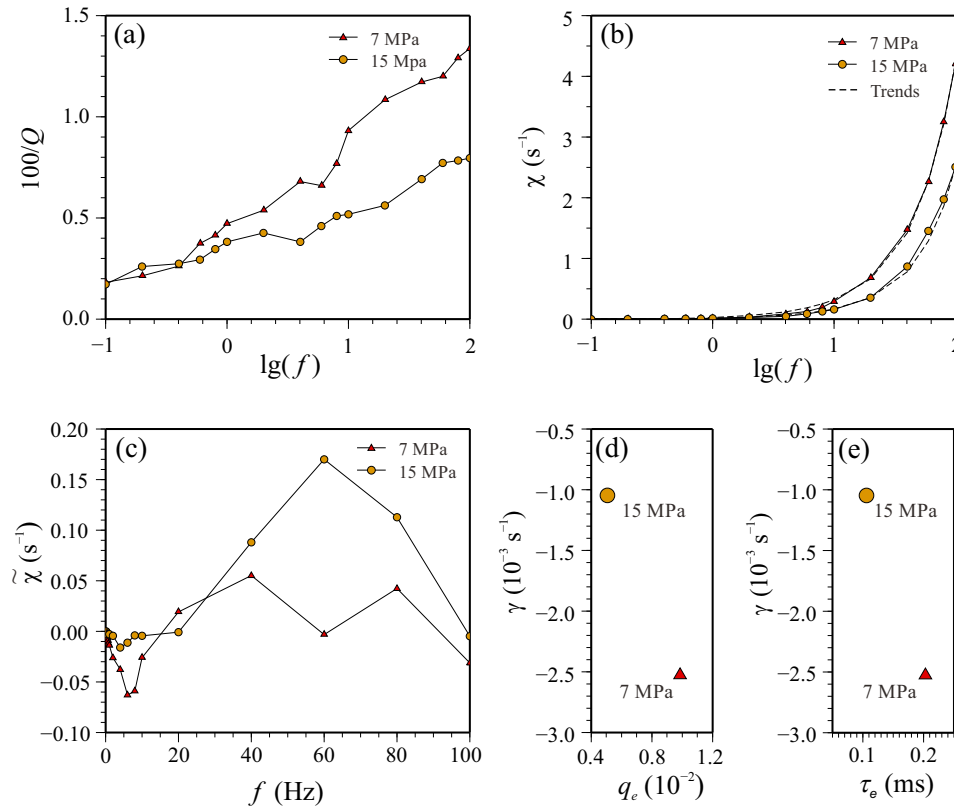
Fig. 4. Young's-modulus attenuation measurements in PMMA plastic at room temperature and axial confining pressures 7 and 15 MPa (legends; Mikhaltsevitch et al., 2016). Panels (a) to (e) are as in Fig. 2.

For Mikhaltsevitch et al. (2016) results with Plexiglas, a transformation of $Q^{-1}(f)$ values into $\chi(f)$ shows that the entire attenuation-coefficient data are well explained by the three functional trend terms in Eq. (5) (Fig. 4(b)). The residual $\tilde{\chi}(f)$ is weak and suggests a small peak near 40 Hz at 7 MPa and a peak at 60 Hz at 15 MPa of axial pressure (Fig. 4(c)). These peaks could correspond to the 3-Hz peak at ambient pressure (noted in the preceding paragraph) moving to higher frequencies. The attenuation equals $q_e \approx 0.01$ at 7 MPa and $q_e \approx 0.005$ at 15 MPa, which is within the range of values for glycerol-saturated sandstone and higher than $q_e \approx 0.002$ for dry sandstone (Fig. 2(d)).

A slight upward curvature of the average trends $\chi(f)$ (positive τ) is seen in Plexiglas data, and the corresponding characteristic times are $\tau_e = 2.0 \times 10^{-4}$ s at 7 MPa axial pressure and 1.1×10^{-4} s at 15 MPa (Fig. 4(e); Eq. (6)). With Young's moduli values from Mikhaltsevitch et al. (2016), the corresponding viscosities are estimated as $\eta_e = 1.1$ MPa·s at 7 MPa axial pressure and 0.85 MPa·s at 15 MPa. These viscosities are close to shear viscosities estimated by Coulman et al. (2013), and they may again be due to thermoelastic mechanical-energy dissipation in a medium with fine-grained thermomechanical properties (Landau and Lifshitz, 1986). Parameters γ are negative and small, similar to other cases considered above.

3.4 Melt-bearing olivine aggregates

A contrasting example of forced-oscillation mechanical testing is given by shear-deformation measurements in mantle rock simulated in synthetic polycrystalline aggregates by Jackson et al. (2004). These experiments focused on attenuation effects caused by partial melts and are interesting to us here because of several new features: Lower frequencies, very high temperatures, and different shapes of the $Q^{-1}(f)$ spectra. In contrast to the Young's modulus experiments in the preceding subsections, shear deformations were produced using torsional stressing of cylindrical samples (Jackson and Paterson, 1993), and the ambient temperatures were much higher. Following Jackson et al. (2004), let us compare one melt-free case (sample 6381 in that paper) and one melt-bearing case (sample 6410; Fig. 5).

In Fig. 5, the $Q^{-1}(f)$ observations with the melt-free and melt-bearing samples are shown after recalculation from functions of oscillation periods by Jackson et al. (2004). Patterns of $Q^{-1}(f)$ are significantly different from the two exploration case examples in this section. Instead of distinct peaks or an increase, the shear-wave $Q^{-1}(f)$ rapidly decreases with frequency. At fixed frequencies, the reported Q^{-1} values also increase with temperature (Fig. 5), which is the same trend as in fluid-saturated sandstone above the relaxation-peak frequencies (Fig. 2(a)). Jackson et al. (2004) referred to these combined frequency and temperature trends as the
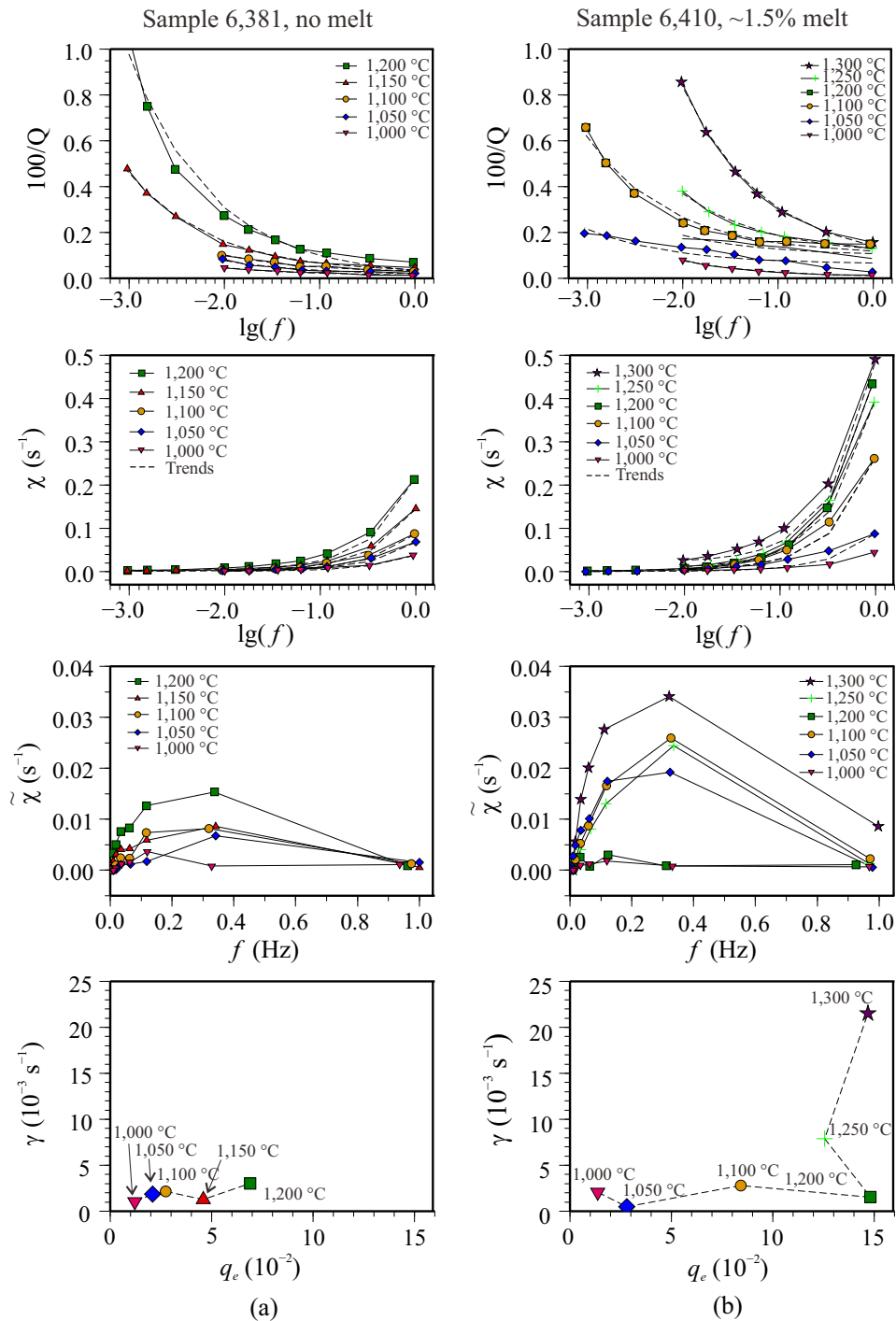
Fig. 5. Torsional attenuation measurements in two samples of polycrystalline olivine aggregates at variable temperatures (legends and labels; Jackson et al., 2004). Columns correspond to (a) samples 6381 and (b) 6410: Measured $Q^{-1}(f)$; the same measurements in $\chi(f)$ form; residual $\tilde{\chi}(f)$; cross-plots of q_e and γ. Dashed lines in the first row show trends $Q^{-1} \propto f^{-1/2} + const$. Dashed lines the second row are the smooth trends due to the first three terms in Eq. (5).

"viscoelastic background" of the material.

Despite the apparent differences in the $Q^{-1}(f)$ data, a transformation into the $\chi(f)$ form reveals a similarity between the melt-free and melt-bearing cases and gives quantitative parameters describing the shapes of the attenuation spectra. First, the shapes of $\chi(f)$ dependencies (second row in Fig. 5) are quite similar to those in Figs. 2(b) through 4(b). The principal contributions to attenuation also come from the linear parts of these dependencies, with q_e ranging from 0.01 at 1,000 °C to 0.07 at 1,300 °C for the melt-free sample (bottom left in Fig. 5), and from $q_e \approx 0.02$ at 1,000 °C to 0.15 at 1,300 °C for the melt-bearing sample (bottom right in Fig. 5). Thus, the melt-bearing material should show an about twice stronger attenuation in a seismic wave. Parameter τ (Eq. (5)) cannot be reliably estimated from these data, but τ_e inferred from q_e (Eq. (6)) increases from 26 ms at 1,000 °C to 140 ms at 1,200 °C for the melt-free sample and from 28 ms at 1,000 °C to 260-320 ms at 1,200-1,300 °C for the melt-bearing sample. These values are an order of magnitude larger than those for glycerol-saturated sandstone at near-room temperatures.

With constant shear modulus 5 GPa of the material (Jackson et al., 2004), solid viscosities η_e are proportional to τ_e and range from 140 MPa·s at 1,000 °C to 1.45 GPa·s at 1,200-1,300 °C. These viscosities are also two to five times larger than viscosities of glycerol-saturated sandstone (Fig. 2(e)). Thus, similar to the case of subsection 3.1, although the viscosity of melt decreases with temperature, the effective viscosity of the rock strongly increases with it. This anti-correlation of the effective and pore-fluid viscosities similarly occurs because of recording at frequencies far above the peaks.

Plots of $\tilde{\chi}(f)$ for the two samples (third row in Fig. 5) show similar spectra with peak levels about twice higher for the melt-bearing sample. The data suggest an attenuation peak near 0.12 Hz at temperature 1,000 °C and possibly a peak near 0.35 Hz at higher temperatures. However, the latter peak occupies the whole measured frequency range, and it could be accommodated by selecting a different nonlinear shape of the average trend.

The reversed lower-frequency "background" trends of $Q^{-1}(f)$ for olivine aggregates (Fig. 5, compared to Figs. 2(a), 3(a), and 4(a)) are due to larger and positive values of parameter $\gamma \approx 0.01$ to 0.03 s^{-1} for the melt-free sample and $\gamma \approx 0.03$ to 0.2 s^{-1} for the melt-bearing sample (compare Figs. 2(d), 3(d), and 4(d) with bottom row in Fig. 5). In the traditional viscoelastic terminology, the observed shapes of $Q^{-1}(f)$ can be attributed to a "relaxation mechanisms" with extremely low frequencies below 1 mHz. Such slow relaxation and amplitude decay could again be due to temperature gradients, thermal dissipation, and thermoelastic effects on the scale of the entire rock sample. Overall, as argued by Morozov et al. (2018), attributing such phenomena to abstract time- and frequency dependencies of phenomenological viscoelastic parameters is an unreliable and physically insufficient approach.

Our selection of parameters γ and q_e in Eq. (5) by linear regression at each temperature is empirical and dictated by simplicity and applicability to other studies of $\chi(f)$ in laboratory and field experiments. However, specifically for high-temperature experiments with olivine aggregates, alternate parameterizations could be useful. In particular, background trends $Q^{-1}(f) \propto f^{-1/2}(\chi(f) \propto \sqrt{f})$ approximate the data remarkably closely (dashed lines in the first row in Fig. 5), suggesting the thermoelastic mechanism of mechanical-energy dissipation. Jackson et al. (2004) described the $Q^{-1}(f)$ background at all temperatures by using an elaborate semi-empirical model with four adjustable parameters. To characterize the shapes of the background functions, these authors defined an empirical time-dependent compliance function in the form of the Andrade law $J(t) = J_U + \beta t^n + t/\eta$ (with empirical parameters β, n, and η), transformed it into the frequency domain, and evaluated the inverse Q as $Q_B^{-1}(f) = \mathrm{Im}\, J(f)/\mathrm{Re}\, J(f)$. Further, frequency f in this function was replaced with a temperature-scaled pseudo-frequency using an Arrhenius-law type relation $f_T = f \exp\left[\left(T^{-1} - T_r^{-1}\right) E_B/R\right]$, where T is the temperature, T_r is some reference temperature at which $f_T = f$, R is the molar gas constant, and E_B is another adjustable parameter interpreted as the activation energy.

Multiple parameterizations can also be selected for the residual frequency dependencies $\tilde{\chi}(f)$. Jackson et al. (2004) used a Gaussian peak in the log-frequency domain superimposed on the $Q_B^{-1}(f_T)$ background, with three additional empirical parameters: Logarithm of the central f_T, variance, and magnitude of the peak. In the present work, in all cases in third row in Fig. 5, and also Figs. 2(c) and 3(c), the broad peaks in $\tilde{\chi}(f)$ could be approximated quite accurately by adding non-polynomial functional forms with one or two additional parameters in Eq. (5). Such terms would allow empirical fitting of the entire $\chi(f)$ dependences (Figs. 2(b), 3(b) and second row in Fig. 5) with accuracy sufficient for all applications.

Comparing the results for the melt-free and melt-bearing samples, Jackson et al. (2004) argued that the presence of melt is indicated by a stronger Gaussian (in the $\log(f_T)$ domain) peak in their model. In the attenuation-coefficient parameterization, this point appears to stand out even stronger, and also with more detail. The shapes of the spectra for the two cases are similar (the middle two rows in Fig. 5), but the melt-bearing case is clearly indicated by about five times larger γ, three times larger q_e (bottom row in Fig. 5) and also twice higher peaks in at all temperatures except 1,000 and 1,200 °C (third row in Fig. 5). Thus, the proposed simple identification of the low-order functional terms (Eq. (5)) is clearly sensitive to the presence of melts within these synthetic mantle rocks.

4. Discussion

The principal observation of this paper is that when interpreting forced-oscillation data, it is useful to not only report the $Q^{-1}(f)$ spectra and identify their peaks but also to quantitatively analyze the attenuation coefficient $\chi(f)$. The same recommendation for many types of field seismic data was made by Morozov (2008, 2010a, 2010b) and Ahmadi and Morozov (2013). The $\chi(f)$ is the primary quantity originating from the fundamental definition of wave attenuation (Eq. (1)), but the $Q^{-1}(f)$ is a secondary and more subtle quantity. The inverse quality factor $Q^{-1}(f)$ possesses an enhanced sensitivity to the low-frequency interval in which various

adverse factors like inaccurate zero-frequency ("geometrical spreading", GS) corrections or thermoelastic effects may be significant.

The key advantage of the $\chi(f)$ parameterization of field or laboratory data is in its freedom from two assumptions implied in the $Q^{-1}(f)$ approach: 1) That χ must equal zero in the low-frequency limit (i.e., that $\gamma = 0$), and 2) that the rock sample and the measurement apparatus obey the viscoelastic theory. In principle, value $\gamma = 0$ can always be achieved by selecting an accurate GS model matching the limit $\gamma = \chi(f \to 0)$ (Eq. (1)). However, in practice, this selection is usually unachievable, and simplified GS models are used, leading to spurious trends and instabilities in the values of $Q^{-1}(f)$. The advantage of the $\chi(f)$ parameterization is that in this form, the inaccuracy of GS becomes clear and can be corrected for (Morozov, 2008, 2010a). In laboratory rock physics, this issue of $\gamma \neq 0$ appears to be less significant, but it still needs to be kept in mind, particularly at low frequencies, high temperatures, or possibly for shear deformations (last case in section 3). More applications are needed to assess the range of γ values for laboratory experiments.

Measurement of a $\chi(f)$ dependence yields a hierarchy of parameters γ, q_e, and τ_e and $\tilde{\chi}(f)$, of which the first three are practically unnoticeable in conventional $Q^{-1}(f)$ parameterizations. By switching to the $\chi(f)$ parameterization, the focus of data analysis shifts from investigating the details of $\tan\delta$ spectra assuming a perfectly accurate zero-attenuation model to measuring the quantitative parameters γ, q_e, and τ_e without such assumptions. In contrast to $Q^{-1}(f)$ (i.e., $\tan\theta$) and parameter γ which may be sensitive to the detail of the present apparatus, parameters q_e, and τ_e (and η_e) are expected to relate to a wave *insitu*, i.e. to the primary object of seismic investigation. Due to their frequency-band averaged characters, parameters γ, q_e, and τ_e should be relatively stable with respect to experimental errors and other adverse factors, since the random noise can be averaged out. However, it is important to note that systematic errors cannot be eliminated by this approach or any another theoretical approaches, and corrections must be made to the experimental setup itself.

Peaks of "wave attenuation" are of primary interest in rock physics and seismic studies; however, shall one look for peaks of functions $Q^{-1}(f)$, $\chi(f)$, or $\tilde{\chi}(f)$? Function $\chi(f)$ usually has no localized peaks (e.g., Fig. 1(c)), and peaks in $\tilde{\chi}(f)$ occur at higher frequencies and are generally less pronounced than those of $Q^{-1}(f)$ (e.g., Fig. 2(b)). Both $\tilde{\chi}(f)$ and $Q^{-1}(f)$ peaks can be used for building detailed models of the medium (Chen et al., 2021); however, $\tilde{\chi}(f)$ might be preferable because this function is free from biases due to insufficiently known GS and/or thermoelastic backgrounds.

In this paper, no formal estimates of the uncertainties are made for quantities γ, q_e, and τ_e. Our key points are clear without error analysis: These quantities are instructive, correlated with physical conditions of the experiments, often nonzero, and yet they are not considered in conventional interpretations of $Q^{-1}(f)$ spectra. Error analysis can be performed using standard methods; however, the principal sources of uncertainties should be related to the limited frequency bands of the data. The residual attenuation coefficient $\tilde{\chi}(f)$ was also only analyzed qualitatively, but this analysis can be extended, yielding additional quantitative parameters. The broad peaks in $\tilde{\chi}(f)$ seen in most cases show that non-polynomial frequency dependencies such as the thermoelastic $\chi(f) \propto \sqrt{f}$ can in some cases be fit to the observed $\chi(f)$ more effectively. Non-polynomial frequency dependencies of $\chi(f)$ could also indicate non-Newtonian internal mechanical friction within the medium (Coulman et al., 2013).

Finally, note that similarly to $Q^{-1}(f)$ and the dynamic modulus $M(f)$, the attenuation coefficients $\chi(f)$ (temporal) and $\alpha(f)$ (spatial) are not strictly material properties for a given rock sample. These quantities can be interpreted as properties of a traveling harmonic wave which would be observed in a (hypothetical) boundless volume of the same material. In the sense of such reference to an idealized case of a homogeneous medium, these properties can be called "apparent attenuation," similarly to the apparent resistivity in electrical surveying (Morozov and Ahmadi, 2015). For detailed interpretation, a significant effort of modeling and inversion is required for removing the effects of experimental conditions and determining the true material properties of the sample. These true material properties would be not the empirical $Q^{-1}(f)$, $\chi(f)$, or $M(f)$ but frequency-independent matrices of elastic, viscous, and Darcy-type friction properties of the medium (Morozov et al., 2018; Chen et al., 2021). For fluid-saturated rock at variable temperatures, this inversion for material properties represents a complex task because of the variety of boundary and thermal conditions in the experiments.

5. Conclusions

Attenuation-coefficient parameterization of forced-oscillation mechanical testing of rock samples is applied to published measurements with glycerol-saturated Berea sandstone, bitumen sands, Plexiglas, and synthetic olivine aggregates at variable temperatures. The parameterization reveals three new attributes which characterize the rock and relate to its physical properties:

1) The effective geometrical (frequency-independent) attenuation denoted γ. This parameter is small and appears negligible for glycerol-saturated sandstone and Plexiglas. However, values $\gamma \approx 2 \times 10^{-3} - 2 \times 10^{-2}$ s^{-1} are significant in lower-frequency, high-temperature torsional-deformation experiments with olivine aggregates. Under these conditions, this effective attenuation is likely cause by thermoelastic relaxation at the surfaces of rock samples.

2) Effective attenuation q_e, which is a counterpart of the conventional frequency-independent inverse Q-factor used in field data analysis. The q_e increases in the presence of pore fluids or melts and with increasing temperature, and it decreases with confining pressure. For Berea sandstone, $q_e \approx 0.002$ for dry rock and $q_e \approx 0.01 - 0.02$ for glycerol-saturated rock. Notably, for fluid-saturated porous rock, attenuation qe decreases with increasing viscosity of the pore fluid. For bitumen sand, the attenuation is much stronger, with $q_e \approx 0.1$ for shear deformation and $q_e \approx 0.15$ for bulk deformation.

3) Characteristic time τ_e or effective viscosity η_e. These parameters are often difficult to differentiate from q_e, but they are closely related to physical properties of the material. From the data of this paper for Plexiglas, η_e = 1.1 MPa·s at 7 MPa and decreases with confining pressure. For dry Berea sandstone, $\eta_e \approx$ 7 MPa·s, and for glycerol-saturated sandstone $\eta_e \approx$ 27, 63, and 70 MPa·s at temperatures of 23 °C, 31 °C, and 37.5 °C, respectively.

Parameters γ, q_e, and τ_e are directly related to the properties of seismic waves in the field and quantities measured in many other experiments in observational and exploration seismology. In addition to these first-order parameters, secondary variations of the attenuation coefficient with frequency are also obtained, and they can be used for obtaining detailed constraints on rock rheology. The study also found that observations of shear forced-oscillation deformations (Jackson et al., 2004) at high temperature may be dominated by thermoelastic mechanical-energy dissipation on the surfaces of the samples.

By using this new attenuation-coefficient parameterization, more useful information can be obtained by analyzing seismic attenuation for conventional and unconventional hydrocarbon exploration.

Acknowledgements

Conflict of interest

The authors declare no competing interest.

References

Ahmadi, A. B., Morozov, I. B. Anisotropic frequency-dependent spreading of seismic waves from first-arrival vertical seismic profile data analysis. Geophysics, 2013, 78(6): C41-C52.

Aki, K., Chouet, B. Origin of coda waves: Source, attenuation, and scattering effects. Journal of Geophysical Research, 1975, 80(23): 3322-3342.

Aki, K., Richards, P. G. Quantitative Seismology, Sausalito, USA, University Science Books, 2002.

Anderson, D. L., Kanamori, H., Hart, R. S., et al. The Earth as a seismic absorption band. Science, 1977, 196(4294): 1104-1106.

Cheng, N. S. Formula for the viscosity of a glycerol-water mixture. Industrial & Engineering Chemistry Research, 2008, 47(9): 3285-3288.

Chen, S., Wen, X., Morozov, I. B., et al. Macroscopic non-Biot's material properties of sandstone with pore-coupled wave-induced fluid flows. Geophysical Prospecting, 2021, 69(3): 514-529.

Coulman, T., Deng, W., Morozov, I. B. Models of seismic attenuation measurements in the laboratory. Canadian Journal of Exploration Geophysics, 2013, 38: 51-67.

Deng, W., Morozov, I. B. Solid viscosity of fluid-saturated porous rock with squirt flows at seismic frequencies. Geophysics, 2016, 81(4): D395-D404.

Deng, W., Morozov, I. B., Fu, L. Y., et al. An extended continuum-mechanics standard linear solid rheology for fluid-saturated porous rock. Geophysical Journal International, 2024, 238(1): 1-14.

Geertsma, J., Smit, D. C. Some aspects of elastic wave propagation in fluid-saturated porous solids. Geophysics, 1961, 26(2): 161-181.

Gurevich, B., Makarynska, D., de Paula, O. B., et al. A simple model for squirt-flow dispersion and attenuation in fluid-saturated granular rocks. Geophysics, 2010, 75(6): N109-N120.

Jackson, I., Faul, U. H., Fitz Gerald, J. D., et al. Shear-wave attenuation and dispersion in melt-bearing olivine polycrystals: 1. Specimen fabrication and mechanical testing. Journal of Geophysical Research: Solid Earth, 2004, 109: B06201.

Jackson, I., Paterson, M. S. A high-pressure, high-temperature apparatus for studies of seismic wave dispersion and attenuation. Pure and Applied Geophysics, 1993, 141: 445-466.

Lakes, R. S. Viscoelastic Materials. Cambridge, England, Cambridge University Press, 2009.

Landau, L. D., Lifshitz, E. M. Theory of Elasticity. Berlin, Germany, Springer Science & Business Media, 1986.

Lomnitz, C. Linear dissipation in solids. Journal of Applied Physics, 1957, 28(2): 201-205.

Mikhaltsevitch, V., Lebedev, M., Gurevich, B. Validation of the laboratory measurements at seismic frequencies using the Kramers-Kronig relationship. Geophysical Research Letters, 2016, 43(10): 4986-4991.

Morozov, I. B. Geometrical attenuation, frequency dependence of Q, and the absorption band problem. Geophysical Journal International, 2008, 175(1): 239-252.

Morozov, I. B. On the causes of frequency-dependent apparent seismological Q. Pure and Applied Geophysics, 2010a, 167: 1131-1146.

Morozov, I. B. Attenuation coefficients of Rayleigh and Lg waves. Journal of Seismology, 2010b, 14(4): 803-822.

Morozov, I. B. Mechanisms of geometrical seismic attenuation. Annals of Geophysics, 2011, 54(3): 235-248.

Morozov, I. B., Ahmadi, A. B. Taxonomy of Q. Geophysics, 2015, 80(1): T41-T49.

Morozov, I. B., Deng, W. Inversion for Biot-consistent material properties in subresonant oscillation experiments with fluid-saturated porous rock. Geophysics, 2018, 83(2): MR67-MR79.

Morozov, I. B., Deng, W., Cao, D. Mechanical analysis of viscoelastic models for Earth media. Geophysical Journal International, 2020, 220(3): 1762-1773.

Morozov, I. B., Jhajhria, A., Deng, W. On strong positive frequency dependencies of quality factors in local-earthquake seismic studies. Pure and Applied Geophysics, 2018, 175: 2595-2607.

Nowick, A. S., Berry, B. S. Subject Index, in Anelastic Relaxation in Crystalline Solids. edited by A. S. Nowick and B. S. Berry, Academic Press, Cambridge, pp. 670-677, 1972.

Pimienta, L., Fortin, J., Guéguen, Y. Bulk modulus dispersion and attenuation in sandstones. Geophysics, 2015a, 80(2): D111-D127.

Pimienta, L., Fortin, J., Guéguen, Y. Experimental study of Young's modulus dispersion and attenuation in fully saturated sandstones. Geophysics, 2015b, 80(5): L57-L72.

Spencer, J. W. Stress relaxations at low frequencies in fluid-saturated rocks: Attenuation and modulus dispersion. Journal of Geophysical Research: Solid Earth, 1981, 26(B3): 1803-1812.

Spencer, J. W. Viscoelasticity of Ells River bitumen sand and 4D monitoring of thermal enhanced oil recovery processes. Geophysics, 2013, 78(6): D419-D428.

Tan, W., Müller, T. M., Ba, J., et al. Drained-to-undrained transition of bulk modulus in fluid-saturated porous rock induced by dead volume variation. Geophys, Prospect, 2020, 68(8): 2494-2503.

Tisato, N., Madonna, C., Boutareaud, S., et al. A new instrumentation to measure seismic waves attenuation. AGU Fall Meeting Abstracts, 2010, 1: 1464.

White, J. E. Biot-Gardner theory of extensional waves in porous rods. Geophysics, 1986, 51(3): 742-745.

Yang, X., Lay, T., Xie, X. B., et al. Geometric spreading of P_n and S_n in a spherical Earth model. Bulletin of the Seismological Society of America, 2007, 97(6): 2053-2065.